Eur. Phys. J. Plus (2024) 139:399
https://doi.org/10.1140/epjp/s13360-024-05189-w

THE EUROPEAN PHYSICAL JOURNAL PLUS

Regular Article

Photoionization treatment of encompassed plasma-implanted exotic atoms

Mustafa Kemal Bahar[a]

Department of Physics, Faculty of Science, Sivas Cumhuriyet University, 58140 Sivas, Turkey

Received: 23 March 2024 / Accepted: 17 April 2024

Abstract This work chews over exotic systems embedded in a non-ideal classical plasma (NICP) under impenetrable spherical confinement, including μH, $(\mu\text{He})^{+}$, and $(\mu\text{Li})^{++}$ systems within a nonrelativistic formalism. The photoionization processes of exotic atomic systems are thoroughly analyzed for different values of the NICP's plasma screening parameter, hence plasma temperature and density, and the radius of spherical confinement. In each case, the energy levels of exotic systems are shown and interpreted in terms of their characteristics. The heavy nature of the muon significantly influences the entire process. Additionally, observable outcomes of different attraction effects originating from the nucleus in muonic systems on both the spectrum and photoionization are identified. The short lifetimes of relevant exotic systems due to the muon and the high bound state energies resulting from the strong attraction energy of the muon significantly inconvenience the photoionization process. However, these disadvantages can be overcome thanks to NICP and spherical confinement, thereby facilitating experimental applications. Important findings regarding these facilitation processes are presented in the present work.

1 Introduction

Muons are one of the significant players in particle physics; they have the same charge as an electron but approximately 207 times more mass. Muons are not only important in fundamental particle physics and cosmology, but also in the field of atomic physics. Muons, which can naturally be found in cosmic rays, can also be produced in laboratory environments. Muons can be used particularly to investigate the structures of chemical bonds and molecular behaviors [1, 2]. Muons can behave like neutrons in various atomic and molecular systems. It has been demonstrated that muons, particularly when inserted into hydrogen, serve as a valuable tool for studying molecular processes, enabling a deeper understanding of the dynamics and structures of chemical bonds [3]. This has the potential for use in molecular spectroscopy and chemical kinetics. Such research could have significant applications in fields such as materials science and the pharmaceutical industry. Muons are particles with a spin-1/2 that can be implanted into various dense mediums and interact with atoms in their local surroundings. Measuring the motion and relaxation of a muon helps understand its interaction with its environment, providing valuable insights into the static and dynamic properties of materials. This enables the development of techniques such as muon spin spectroscopy and allows for a deeper analysis of material properties [4]. Muonic exotic atoms are defined as special atomic structures formed when a muon is present within an atomic system. In these atoms, instead of an electron orbiting the nucleus as usual, a muon becomes trapped in the nucleus. Due to the muon's heavier mass compared to an electron, muonic exotic atoms represent an important research topic in atomic physics. Studying muonic exotic atoms implies that atomic spectra may differ from those of normal atoms [5]. This situation provides a fundamental opportunity, particularly for better understanding atomic and molecular structures. Additionally, muonic exotic atoms play an important role in fundamental particle physics and nuclear physics as well [6]. These atoms play a critical role in research, especially aimed at understanding the internal structure of atomic nuclei and weak interactions. In this context, muonic exotic atoms constitute a significant focal point of studies in the field of atomic physics [7]. Despite their short lifetimes, muonic exotic atoms are considered as an important research area in various scientific disciplines. These atoms have various applications in fields such as particle physics, nuclear physics, atomic and molecular physics, materials science, among others. In research on fundamental particle physics, muonic exotic atoms can be utilized to better understand the fundamental concepts of particle physics and to discover new phenomena [8]. In the field of atomic and molecular physics, these atoms can enable a deeper understanding of atomic structures and molecular dynamics [9]. In nuclear physics research, muonic exotic atoms can be a valuable tool for providing more information about nuclear structure and interactions [10]. From the perspective of materials science, these atoms can facilitate the design and synthesis of new materials by studying their effects on the structure and properties of materials [11]. Also, recently, muonic atoms have played an important role in lasers [12]. Therefore, muonic exotic atoms are considered an important research tool in various scientific research fields despite their short lifetimes.

[a] e-mail: mussiv58@gmail.com (corresponding author)

Published online: 09 May 2024

In the present work, we probe the relevant muonic systems under a spherical confinement. But why a confinement? It was understood that the removal of the degeneracy of a system's energy and angular momentum states through the application of symmetry constraints is an important quantum mechanical feature beyond atoms and molecules. As a result, the Jahn–Teller effect has also been utilized to explain the superconductivity of metals. The subject of constrained atomic and molecular systems is broad. The results range from the formation of white dwarfs and neutron stars on one hand to the transformation of insulators into metals and graphite into diamond on the other. The properties of atoms, molecules and materials change under constraint. Understanding them means making the best use of the numerous opportunities they provide. Fullerenes, zeolites, cage effects for photochemists, and matrix isolation techniques used to study atoms and molecules in isolation for spectroscopists aim to obtain and utilize the significant consequences of confinement [13]. Due to the highly significant effects of confinement, the relevant muonic systems in the present work are viewed under the effect of spherical confinement. Confining muonic atoms is important in many respects, as mentioned above, and perhaps the most significant advantage is the ability to control them. Spatial confinement of muonium atoms is experimentally feasible. Khaw et al. [14] have demonstrated that vacuum-diffused muonium undergoes reflection between two SiO_2 bounding surfaces spaced 1 mm apart. The reflection probability on the bounding surfaces maintained at 100 K was determined to be approximately 90%, and the reflection process could be described by the cosine law. This technique represents a significant step toward conducting new experiments with exotic atomic systems and toward measuring the $1S - 2S$ transition frequency using continuous-wave laser spectroscopy. When compared to electrons, muons move in orbits much closer to the nucleus and experience a significantly increased binding energy. The changes in the ground-state energy of muonic systems such as H, He^+, and Li^{+2} under high compression have been investigated, taking into account the nuclear mass and the finite volume with uniformly distributed charge of the nucleus. The findings indicate that the maximum energy correction becomes more pronounced with increasing compression and mass of the atomic nucleus [15]. Various three-particle systems involving muons, or Borromean correlated three-particle molecular systems, are significant for fundamental particle physics, many-body studies, nuclear physics, cold atom physics, and chemical bond analysis. They enable the development of new mathematical and theoretical models and can lead to various technological applications. The Borromean states and resonant states of molecular ions under the effect of exponential cosine screened Coulomb potential, such as $pp\mu$, $dd\mu$, and $tt\mu$, have been theoretically investigated [16]. In this study, critical values of the screening parameter for Borromean correlations are reported. Modern experimental techniques now allow the investigation of certain bound state properties of most exotic atomic systems. Few-particle muonic atomic systems are included in this. All atomic and molecular few-particle systems containing a positively charged muon and two electrons have significantly different electron density distributions from normal 'similar' atomic and molecular systems. In fact, such systems can be thought of as a separate class of bound systems that are neither atoms nor molecules. The calculation of some matrix elements of such two-, three-, or four-particle systems involves the disappearance of electron-positron pairs in the structure, and the analysis of hyperfine structure has been performed [17]. There are indeed numerous experimental studies on muonic systems, and the motivations behind each of them are quite diverse and purposeful. Some of these include the observation of long-lived muonic hydrogen in the 2 S state [18] and laser excitation of the $1s$-hyperfine transition in muonic hydrogen [19], which respectively explain the lifetime of muonic hydrogen and how the laser spectroscopy process can be optimized.

The influence of plasma environments has been investigated in muonic atomic systems, similar to other atomic systems. Plasmas are important for muonic exotic atoms because the plasma environment can alter or affect the properties of muonic atoms. Muonic atoms within plasmas at high temperatures and densities can undergo interactions that affect electron distribution and may play a role in nuclear fusion research. Additionally, the plasma environment can be utilized as a tool to study the behavior of muons, and laser-plasma interactions offer a potential method to control the properties of muonic atoms. However, the short lifetime of muons and the higher bound state energies, compared to electrons, in muonic hydrogenic systems make ionization of muons and measurements during the ionization process challenging. Plasmas provide the most favorable environment for exciting any atom to emit radiation. In this context, muonic systems are often studied in Debye plasmas. In a Debye plasma, the effects of plasma screening parameters, nuclear size, and mass effects on the isotope shifts of bound state energies, radial probability densities, transition energies, and binding energies of embedded muonic hydrogen-like atoms have been investigated within a perturbative framework [20]. The potential energy of Coulombically bound $p^+\mu^-$ and $\mu^+\mu^-$ exotic atoms has been modified by the Debye plasma environment, and the energy levels and structural properties of these exotic atoms, confined in a spherical box, have been investigated. The effect of plasma and confinement on system properties such as orbital energies, excited states, dipole polarizabilities, oscillator strengths, and transition probabilities has been studied using time-dependent perturbation theory [21]. The effect of the Debye plasma environment on the ground-state energies of exotic systems such as $pp\mu$, $dd\mu$, and $tt\mu$ has been investigated within a generalized three-particle formalism using multi-term correlated basis sets [22]. In this study, the effect of the Debye plasma on structural properties as well as the correlation between particles on binding has been analyzed. Similarly, as another study, the influence of plasma screening and particle correlations on the electron affinity of exotic systems such as muonium (μ^+e^-) and pionium (π^+e^-) under the shielding effect of Debye plasma has been investigated. [23]. In a Debye plasma environment, the bound and resonance states of $td\mu$, $dd\mu$ exotic molecular ions have been elucidated using accurate correlated basis functions, and the effects of the plasma on the states have been demonstrated [24]. The most significant common result of such studies in plasma environments is that plasma environments create significant changes in the structural, electronic, and spectroscopic properties of exotic systems, and these changes are controllable. To the best of our knowledge, the most commonly used plasma environment for the structural properties of exotic atoms is the Debye plasma. The new information and opportunities provided by Debye plasma

serve as a good motivation for the investigation of other plasma types. In this regard, the plasma environment to be considered in the present work is the non-ideal classical plasma (NICP). However, in order to better understand the results of NICP in the present study, the results related to Debye and quantum plasma are compared with those of NICP. Non-ideal classical plasma is a version of the classical plasma model that deviates from the ideal condition and takes into account the more complex conditions in the real world. Classical plasma occurs when gas molecules ionize under high-temperature and low-density conditions. In partially ionized plasma, if the temperature and particle density are low, the interaction between ions, electrons, and atoms that make up the plasma is weak [25]. The ideal classical plasma models situations where interactions between plasma particles are negligible. However, in real applications, interactions between plasma particles can be significant, and therefore non-ideal plasma models are used. Transitioning from the ideal scenario to real plasma applications requires increasing the plasma density. This is because increased particle density strengthens the interparticle interactions and leads to plasma non-ideality. The ratio of the average energy of interparticle interactions to the average thermal kinetic energy is a dimensionless parameter, denoted as γ, which serves as a reference for plasma non-ideality [25, 26]. Non-ideal classical plasma offers some advantages compared to other types of plasma: due to non-ideality, it is more suitable for real-world applications. It surpasses the limits of ideal plasma models under high-temperature and low-density conditions, thus enabling a better understanding of plasma's thermal behavior. Additionally, it may be more suitable for various applications such as high-density plasma systems and stellar interiors. Finally, non-ideal classical plasma models offer potential for further research due to their suitability for real-world plasma applications, enabling a more detailed examination of the thermodynamic, conductivity, and other properties of plasma [27]. Prasad et al. have compared the multiple polarizabilities and generalized oscillator strengths of the H atom in non-ideal classical plasma under spherical confinement using the eighth-order finite difference method, providing comparison with Debye plasma effects [28]. Some of the most recent theoretical studies on non-ideal classical plasma are as follows: The polarizabilities of hydrogen and positronium negative ions embedded in non-ideal classical plasma have been investigated using correlated exponential wave functions. The effects of plasma non-ideality on the ground-state energies and static and dynamic dipole polarizabilities of negative ions have been thoroughly probed over a wide range of non-ideality [29]. A calculation has been conducted to investigate the effects of the non-ideality of classical plasma on the energy levels of hydrogen-like atoms confined in a spherical cage. Energy levels resulting from variations in plasma parameters and cage size have been particularly scrutinized, and it has been explained that increasing plasma non-ideality leads to an elongation of the critical cage size [30]. Calculation of atomic properties in a non-ideal classical plasma and an approach to the electron collision excitation process have been presented based on the relativistic distorted wave methodology. Bound/continuous state wave functions and electron collision excitation matrix elements have been systematically reviewed to consider the effects of plasma non-ideality on electronic structures, radiative properties, and excitation cross sections within a specified range of temperature and density. The results are of fundamental importance, particularly for the analysis of atomic processes in non-ideal plasmas [31]. Moreover, recent studies on endofullerenes embedded in non-ideal classical plasma provide significant findings regarding the energy states, oscillator strengths, dipole polarizabilities, orbital charge-currents and induced magnetic fields, and photoionizations [32, 33]. The most significant common result observed in all such studies is that non-ideal classical plasma screening modifies the localization of bound and continuum states and their energy spectrum, thereby modifying many properties such as electronic, optical, statistical, and spectroscopic characteristics. All processes and outcomes related to this modification are of a manual nature in these studies.

The short lifetimes of muonic hydrogenic systems make quite challenging experimental investigation of their properties such as oscillator strength, polarizability, and photoionization. However, such experiments are now feasible with current technologies. Nevertheless, due to the experimental difficulty and various limitations of such investigations, there is a significant need for theoretical studies. The heavy nature of the muon and its much higher binding energies compared to the electron greatly make difficult the ionization process. Therefore, non-ideal classical plasmas, which form under high temperature and density conditions and play a role in complex systems ranging from space plasmas to thermonuclear fusion reactors, will greatly facilitate the photoionization process. This will somewhat alleviate the short lifetime and the challenge of ionizations, which could be considered as a disadvantage in muonic systems. On the other hand, studying the photoionization process of muonic hydrogenic atoms within non-ideal classical plasma can contribute to understanding exotic atomic interactions and energy transfer in such plasmas. A scrutiny of the photoionization process of muonic hydrogenic atoms in non-ideal plasma contributes to a better understanding of the physical properties of such systems and the development of potential applications. These realities are considerable motivations in the preparation process of the present work. In this context, our expectation from the present work is briefly to provide detailed analysis of the properties, degeneracies, photomuon energy ranges, and PCS characteristics of the μH, $(\mu\text{He})^{+}$, and $(\mu\text{Li})^{++}$ exotic systems' bound and continuum states, along with their responses to plasma parameters and confinement effects, within a causal relationship.

The work is planned as follows: In Sect. 2, the theoretical model and procedure of the physical elucidation are presented. In Sect. 3, the obtained results are explained in detail. The last section is dedicated to summarizing the main findings of the study.

2 Theoretical model and procedure

When constructing the nonrelativistic Hamiltonians of muonic atoms, the coordinates of both the nucleus and the muon's motion are taken into account. In this case, the Hamiltonian is given as follows:

$$H = -\frac{\hbar^2}{2M_N}\nabla_N^2 - \frac{\hbar^2}{2M_\mu}\nabla_\mu^2 - \frac{Ze^2}{|r_N - r_\mu|} + V_{con}(\mathbf{r}_N - \mathbf{r}_\mu), \tag{1}$$

where M_N is the nucleus mass, M_μ is the muon mass, r_N is the position vector of the nucleus, and r_μ is the position vector of the muon. $V_{\rm con}(\mathbf{r}_N - \mathbf{r}_\mu)$ is the spherical confinement potential to encompass the muonic hydrogen-like atoms. Two-body nonrelativistic Hamiltonian separates to center-off mass part and relative muon-nucleus (μN) motion part. The coordinates of center-off mass part and relative μN one are given by

$$\mathbf{R}_{\rm cm} = \frac{M_N\mathbf{r}_N + M_\mu\mathbf{r}_\mu}{M_N + M_\mu}, \tag{2}$$

$$\mathbf{r} = \mathbf{r}_N - \mathbf{r}_\mu. \tag{3}$$

In this case, the Hamiltonian in Eq. 1 can be separated within the motion coordinates ($\mathbf{R}_{\rm cm}$, $\mathbf{r}$):

$$H_T = H_{\rm cm} + H_r, \tag{4}$$

where $H_{\rm cm}$ (the center-off mass Hamiltonian) and H_r (the relative motion Hamiltonian) are given by

$$H_{\rm cm} = -\frac{\hbar^2}{2(M_N + M_\mu)}\nabla_{\rm cm}^2, \tag{5}$$

$$H_r = -\frac{\hbar^2}{2\mu}\nabla_r^2 - \frac{Ze^2}{r} + V_{\rm con}(r), \tag{6}$$

where μ is the reduced mass as

$$\mu = \frac{M_\mu M_N}{M_\mu + M_N}, \tag{7}$$

and the confinement potential $V_{\rm con}(r)$ reads to

$$V_{\rm con}(r) = \begin{cases} 0, & \text{if } r < R_0 \\ \infty, & \text{if } r \geq R_0. \end{cases} \tag{8}$$

with R_0 (the spherical confinement radius). $H_{\rm cm}$ is the Hamiltonian for the free solutions of a system consisting of particles with masses $M_N + M_\mu$, providing only a constant contribution to relevant examinations. The eigenvalue equation that needs to be solved for the investigations of the system is $H_r\Psi = E_r\Psi$. For muonic hydrogen-like atoms under the screening effect of a non-ideal classical plasma, the Coulomb interaction is modified as follows [34]:

$$V_{\rm NICP(H)} = -\frac{\rm Ze^2}{4\pi\varepsilon_0 r} exp(-\frac{r}{\lambda_D})\left[\frac{1+\gamma q(r)}{1+p(\gamma)}\right], \tag{9}$$

with λ_D (the plasma screening parameter), and the relevant quantities are stated as

$$\lambda_D^{-1} = \left(\frac{e^2 n_e}{\varepsilon_0 k_B T_e}\right)^{-1}, \tag{10}$$

$$\gamma = \left(\frac{e^2}{4\pi\varepsilon_0}\right)\frac{1}{\lambda_D k_B T_e}, \tag{11}$$

$$q(r) = \frac{1}{10}\left[exp(\sqrt{\gamma}\lambda_D^{-1}r) - 1\right]\left[1 - exp(2\lambda_D^{-1}r)\right], \tag{12}$$

where n_e, T_e (respectively, the plasma electron density and temperature), ε_0 (the vacuum dielectric constant), e (is the electron charge), $k_{\rm B}$ (the Boltzmann constant). $p(\gamma)$ is the correlation coefficients for a wide range of γ variations ($0 < \gamma \leq 4$), and $p(\gamma)$ formula is produced by utilizing interpolation as follows:

$$p(\gamma) = -0.008617 + 0.455861\gamma - 0.108389\gamma^2 + 0.009377\gamma^3. \tag{13}$$

Then, for non-ideal classical plasma (NICP)-immersed muonic hydrogen-like atoms, the relative Hamiltonian ($H_r = H$) in Eq. 6 transforms to the following form:

$$H = -\frac{\hbar^2}{2\mu}\nabla^2 - \frac{Ze^2}{4\pi\varepsilon_0 r} exp\left(-\frac{r}{\lambda_D}\right)\left[\frac{1+\gamma q(r)}{1+p(\gamma)}\right] + V_{con}(r). \tag{14}$$

In this case, the eigenvalue equation to be solved is $H\psi(r,\theta,\phi) = E\psi(r,\theta,\phi)$, where $\psi(r,\theta,\phi) = R_{n\ell}(r)Y_\ell^m(\theta,\phi) = u_{n\ell}(r)r^{-1}Y_\ell^m(\theta,\phi)$ (being $R_{n\ell}(r)$ is the radial wave functions and $Y_\ell^m(\theta,\phi)$ is the spherical harmonics). In turn, the radial Schrödinger equation can be read in the following formalism:

$$u''_{n\ell}(r) + \frac{2\mu}{\hbar^2}\Big(E_{n\ell} - U_{eff}(r)\Big)u_{n\ell}(r) = 0, \tag{15}$$

where the effective potential $U_{\text{eff}}(r)$ is

$$U_{\text{eff}}(r) = V_{\text{NICP}}(r,\lambda_D,Z) + V_{\text{con}}(r,R_0) + \frac{\hbar^2}{2\mu}\frac{\ell(\ell+1)}{r^2}. \tag{16}$$

We take into consideration the tridiagonal matrix method (TMM) to solve the radial Schrödinger equation [35]. For detail, please refer [35].

For transition from state $\mid n_i\ell_i >^{(i)}$ to state $\mid n_f\ell_f >^{(f)}$, the dipole oscillator strength is given by [36, 37].

$$f_{i\to f} = \frac{2\mu}{3\hbar^2}\Delta E\frac{\ell_{\max}}{2\ell_i+1}(\langle i|r|f\rangle)^2, \tag{17}$$

where $\ell_{\max} = (\max;\ell_i,\ell_f)$ and $\Delta E = E_f - E_i$. Also, it should be provided for transition rule that $\ell_f = \ell_i \pm 1$. The oscillator strength computation is a necessary procedure in the photoionization treatment. In consideration of single transition, the photoionization cross section (PCS) is in the following most general form:

$$\sigma_{n\ell} = \pi^2\left(\frac{e^2\hbar}{2\mu c}\right)\frac{df_{ni}}{\mathrm{d}E}, \tag{18}$$

where $\mathrm{d}f_{ni}/\mathrm{d}E$ is the dipole oscillator strength density for the range between E and $E + \mathrm{d}E$, c is the speed of the light, μ is the reduced mass. The continuum states should be considered due to ionization process nature. The usual normalization of the bound states is expressed as

$$\int_0^{R_0} u_{n'\ell}(r)u_{n\ell}(r)dr = \delta_{n,n'}. \tag{19}$$

In the ionization spectrum, the continuous energy band of continuum wave functions renders the normalization procedure energy-dependent. Then, the normalization condition of the continuum wave functions is given by [37]

$$\int_0^{R_0} u_{E\ell}(r)dr\int_{E-\delta E}^{E+\delta E} u_{E'}(r)\mathrm{d}E' = 1, \tag{20}$$

with δE (the small energy interval). In that case, the dipole oscillator strength density is read by

$$\frac{\mathrm{d}f_{fi}}{\mathrm{d}E} = \frac{2\mu}{3\hbar^2}(E_n - E_i)\langle R_{E_n}(r)|r|R_{E_i}(r)\rangle^2, \tag{21}$$

where $R_{E_n}(r) = u_{E_n}(r)r^{-1}$. We take into consideration the normalization process represented by Ugray in order to be able to normalize the radial wave functions of the continuum spectra [38]

$$R_{E_n}(r) = \sqrt{2}(E_{n+1} - E_{n-1})^{-1/2}R_n(r), \tag{22}$$

where $E_{n\pm1}$ are the energies of the adjacent above-below continuum excited state to E_n, while the $R_n(r)$ is the normalized wave function of the confined muonic atom system. The NICP-immersed muonic hydrogen-like atoms are subject to the potential V_{con} associated with spherical confinement, and the pressure in question is defined as follows:

$$P = (4\pi R_0^3)^{-1}\Big(E_0 - \langle V\rangle\Big) \tag{23}$$

where E_0 is the ground-state energy, $\langle V\rangle$ is the estimated value of potential energy, and R_0 is the spherical confinement radius.

3 Result and discussions

In the present work, the photoionization dynamics of muonic hydrogen atom, helium, and lithium ions embedded in a non-ideal classical plasma (NICP) (and also, for comparison, Debye and quantum plasma environments) confined within a spherical region of radius R_0 are viewed. In this context, there are two important external parameters for the photoionization cross section (PCS): λ (plasma screening parameter) and R_0 (spherical encompassment radius). The parameter λ depends on the plasma density (n_e) and plasma temperature (T_e), and the values of λ considered throughout the study are selected to be consistent with experimental data to provide the NICP environment. Therefore, the values are constrained to intermediate values between $n_e = 1\times10^{24} - 2.5\times10^{26}\mathrm{m}^{-3}$ and $T_e = 10^4 - 10^5\mathrm{K}$. To compare the results, exotic systems μH, $(\mu\mathrm{He})^+$, and $(\mu\mathrm{Li})^{++}$ embedded in a Debye plasma environment

Table 1 Comparison of the ground-state energies (1s) of Debye plasma-immersed muonic hydrogen atom (μH) in keV unit

$\lambda(a_\mu^B)$	Present results	Ref. [20]	Ref. [39]
∞	−2.528362	−2.528362	−2.528362
200	−2.500338	−2.500348	
100	−2.472502	−2.472566	−2.472566
80	−2.458639	−2.458762	
50	−2.417658	−2.417690	−2.417690
40	−2.390512	−2.390590	
20	−2.258314	−2.258386	−2.258386
12	−2.090302	−2.090322	
10	−2.009687	−2.009654	−2.009654
8	−1.892679	−1.892684	−1.892684
6	−1.708029	−1.708036	−1.708036
4	−1.374608	−1.374767	−1.374767
3.8	−1.326102	−1.326282	−1.326282
3.0	−1.085045	−1.085546	−1.085546
2.5	−0.883099	−0.883257	−0.883257

Table 2 2s and 2p energies of Debye plasma-immersed muonic hydrogen atom (μH) in keV unit

$\lambda(a_\mu^B)$	2s	2p
∞	− 0.632090	− 0.632089
	− 0.632090[a]	− 0.632090[a]
	− 0.632090[b]	
200	− 0.604421	− 0.604345
	− 0.604423[a]	− 0.604346[a]
100	− 0.577658	
	− 0.577660[a]	− 0.577360[a]
	− 0.577660[b]	
80	− 0.564602	− 0.564142
	− 0.564607[a]	− 0.564144[a]
50	− 0.526719	
	− 0.526722[a]	− 0.525574[a]
	− 0.526722[b]	
40	− 0.502489	− 0.500732
	− 0.502490[a]	− 0.500735[a]
20	− 0.392740	
	− 0.392742[a]	− 0.386426[a]
	− 0.392742[b]	
10	− 0.222898	− 0.202617
	− 0.222900[a]	− 0.202620[a]
	− 0.222900[b]	
4	− 0.004689	
	− 0.004697[a]	
	− 0.004697[b]	

[a]Quoted from Ref. [20]
[b]Quoted from Ref. [39]

without confinement effects are considered. To make such a comparison, it is sufficient to consider the potential $V_D(r)$ instead of $V_{\mathrm{NICP}}(r)$ in the effective potential $U_{\mathrm{eff}}(r)$ and take the limit $R_0 \to \infty$. In a nutshell, they are read by

$$V_D = -\frac{\mathrm{Ze}^2}{4\pi\varepsilon_0 r}\exp\left(-\frac{r}{\lambda_D}\right), \tag{24}$$

and

$$V_D = -\frac{Ze^2}{4\pi\varepsilon_0 r}\exp\left(-\frac{r}{\lambda_D}\right)\cos(r/\lambda). \tag{25}$$

Table 3 Ground-state energies ($1s$) of Debye plasma-immersed muonic helium $(\mu He)^+$ and lithium atom $(\mu Li)^{++}$ in keV unit

System	$\lambda = \infty$	1s			$\lambda = 10$	$\lambda = 1$
		$\lambda = 100$	$\lambda = 60$	$\lambda = 20$		
$(\mu He)^+$	− 43.759330	− 43.310898	− 43.013900	− 41.551476	− 39.426362	− 12.395239
	− 43.759330[a]	− 43.310899[a]	− 43.013901[a]	− 41.551478[a]	− 39.426364[a]	− 12.395240[a]
$(\mu Li)^{++}$	− 99.284297	− 98.60870	− 98.161659	− 95.949089	− 92.699107	− 46.224880
	− 99.284297[a]	− 98.608671[a]	− 98.161661[a]	− 95.949095[a]	− 92.699110[a]	− 46.224890[a]

[a] Quoted from Ref. [20]

Table 4 First excited energies ($2s$) of Debye plasma-immersed muonic helium $(\mu He)^+$ and muonic lithium atom $(\mu Li)^{++}$ in keV unit

	$\lambda = \infty$	2s		$\lambda = 6$	$\lambda = 4$
		$\lambda = 100$	$\lambda = 20$		
$(\mu He)^+$	− 10.940985	− 10.497744	− 8.854679	− 5.078271	− 3.146599
	− 10.940989[a]	− 10.497748[a]	− 8.854693[a]	− 5.078278[a]	− 3.146687[a]
$(\mu Li)^{++}$	− 24.835031	− 24.166468	− 21.624703	− 15.288121	− 11.615524
	− 24.835034[a]	− 24.166472[a]	− 21.624776[a]	− 15.288135[a]	− 11.615790[a]

[a] Quoted from Ref. [20]

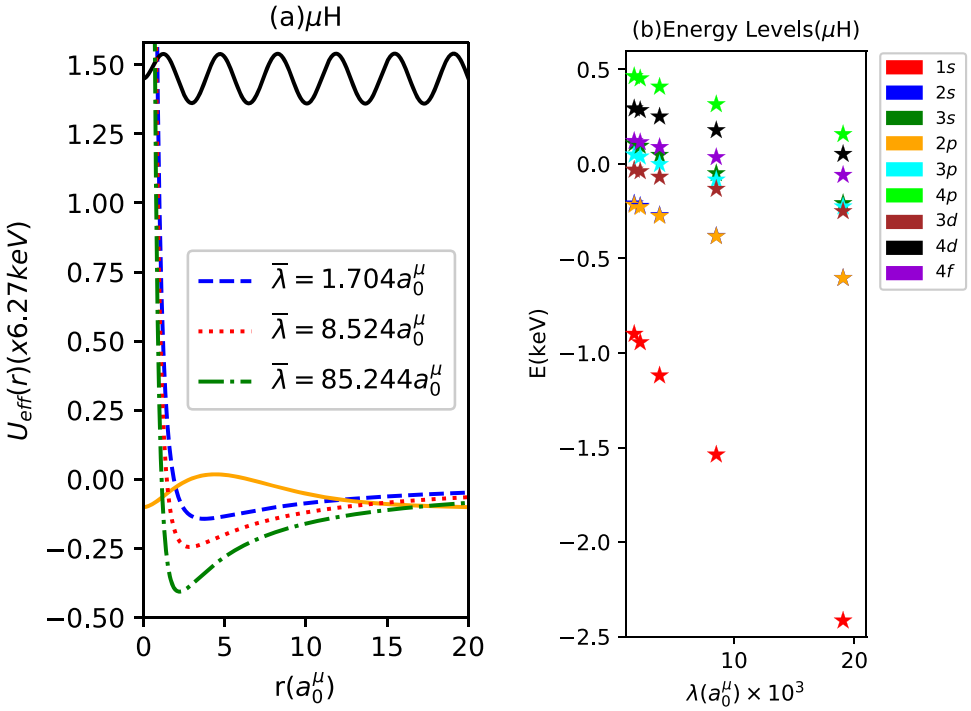

Fig. 1 **a** Effective potential including the radial wave functions of $2p$ and a continuum state, for muonic hydrogen atom (μH) immersed in the non-ideal classical plasma described by the NICP potential with $\bar{\lambda} = 1.704 - 8.524 - 85.244a_0^\mu$, as a function of *r.Note* $\bar{\lambda}$=$\lambda \times 10^{-3}$, $R_0 = 20a_0^\mu$, $\ell = 1$. **b** Some bound and pseudocontinuum state energies for muonic hydrogen atom (μH) immersed in the non-ideal classical plasma as a function of λ

In Table 1, a comparison of the ground-state energies of muonic hydrogen (μH) embedded in a Debye plasma is shown over a wide range of plasma screening parameter λ. In Table 2, a comparison for the $2s$ and $2p$ energies of the same atomic system is presented. In Tables 3 and 4, the ground and first excited state energies of muonic helium $(\mu He)^+$ and muonic lithium $(\mu Li)^{++}$ exotic systems embedded in a Debye plasma environment are presented, respectively. As seen from these tables, there is a very good consistency between the results obtained from the simulations and methodologies of our work and those of the references, which is important for testing the methodology and our current calculation software. Throughout the study, the spherical confinement radius is taken as $R_0 = 20a_0^\mu$, and the $E_{1s} \rightarrow E_c$ (continuum energy) transition is considered for the PCS calculations. The numerical values of all parameters in the present work are physically accessible.

In Fig. 1a, the effective potential profiles with $\ell = 1$ for μH atom embedded in a NICP environment within an impenetrable spherical confinement radius of $R_0 = 20a_0^\mu$ are shown for three different values of λ. Additionally, the $2p$ bound state wave function and a continuum state wave function with an energy of 9.165458 keV are shown within this potential, and these are for $\bar{\lambda} = 1.704a_0^\mu$. Figure 1b illustrates some energy levels for s, p, d, and f states as a function of the plasma shielding parameter λ , while $R_0 = 20a_0^\mu$. As seen in Fig. 1a, the increase in the λ parameter leads to an increase in the strength of the effective potential. Additionally, it is

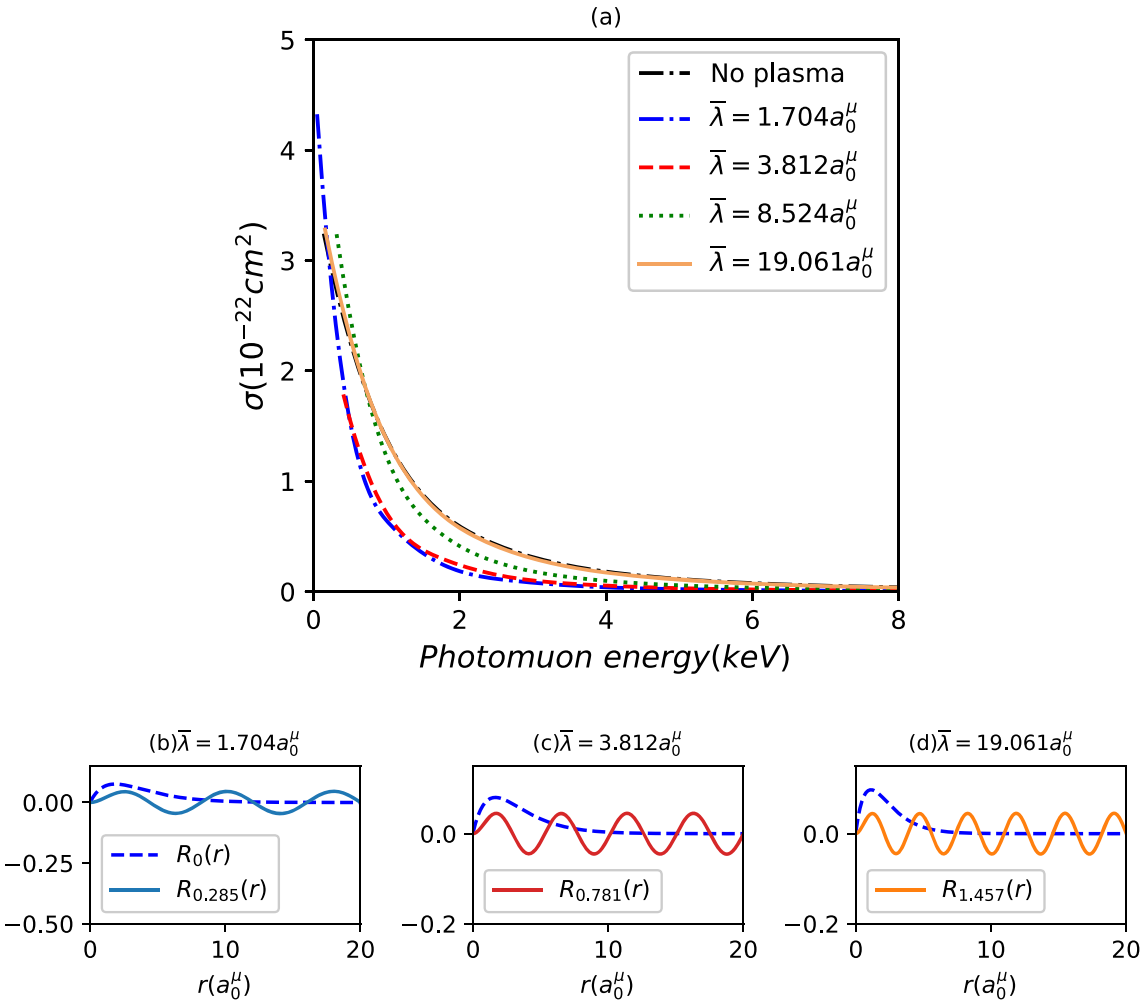

Fig. 2 **a** Photoionization cross sections for μH atom immersed in the non-ideal classical plasma with $\bar{\lambda} = 1.704, 3.812, 8.52, 19.061a_0^\mu$ and free-plasma environment, when $R_0 = 20a_0^\mu$, as a function of photomuon energy. **b**, **c** and **d** The radial wave functions for $1s-$state and continuum states with $\bar{\lambda} = 1.704, 3.812, 19.061a_0^\mu$ as a function of r, where E_n for $R_{E_n}(r)$ is in muonic atomic units (m.a.u.)

observed that the effective potential is relatively stronger at smaller radial distances, which is a determining factor for the localization of bound states. Since the dependence of λ on n_e and T_e is known according to Eq. 10, it can be easily determined how U_{eff} can be adjusted in terms of intensity with plasma temperature and density. With an increase in the λ parameter, it is observed that both bound and pseudocontinuum levels lower in energy (see Fig. 1b). The most affected level is, as expected, the $1s$ level because the muon feels the strongest attraction from the Ze charged nucleus at this level. In Fig. 2a, for four different values of the plasma shielding parameter λ and for the free-plasma environment, the photoionization cross-section (PCS) curves of μH as a function of the photomuon energy are shown when $R_0 = 20a_0^\mu$. As observed, for all considered λ values for μH, the PCS curves exhibit an exponential decrease with increasing photomuon energies. The PCS curves, which are maximum around the ionization threshold, asymptotically approach the energy axis at higher photomuon energies. Low-energy photons provide sufficient energy to remove the bound μ^- from the atom by exerting energy on it. In the μH atom, compared to the hydrogen atom, the muon is closer to the nucleus and has a higher bound state energy. Higher energies are required to ionize μ^-. Therefore, the energy axis is in the keV scale. The reason for the high PCS values at low photomuon energies is due to the muon's greater mass, which allows it to converge the nucleus more closely (186 times closer than the electron) and have more bound state energy. Such a massive muon is not expected to reach high continuum energies after ionization. Therefore, it is expected that the PCS values around the ionization threshold will be highest. However, the involvement of the NICP environment does not alter the exponential decrement character of the photoionization process, but rather shifts the resulting data in an observable manner. It has been found that the effective potential profile in the free-plasma environment (pure Coulomb interaction) is nearly the same as that for $\overline{\lambda} = 85.24420a_0^\mu$ (see Fig. 1a). Therefore, reducing the λ parameter decreases the energy of the bound state energies of the muon in the weakened effective potential, thereby increasing the probability of the photoionization process occurring due to excitation by photons. Hence, as the values of λ decrease, the PCS curves shift toward the ionization threshold region (see Fig. 2a). In other words, the probability of the μ^- in

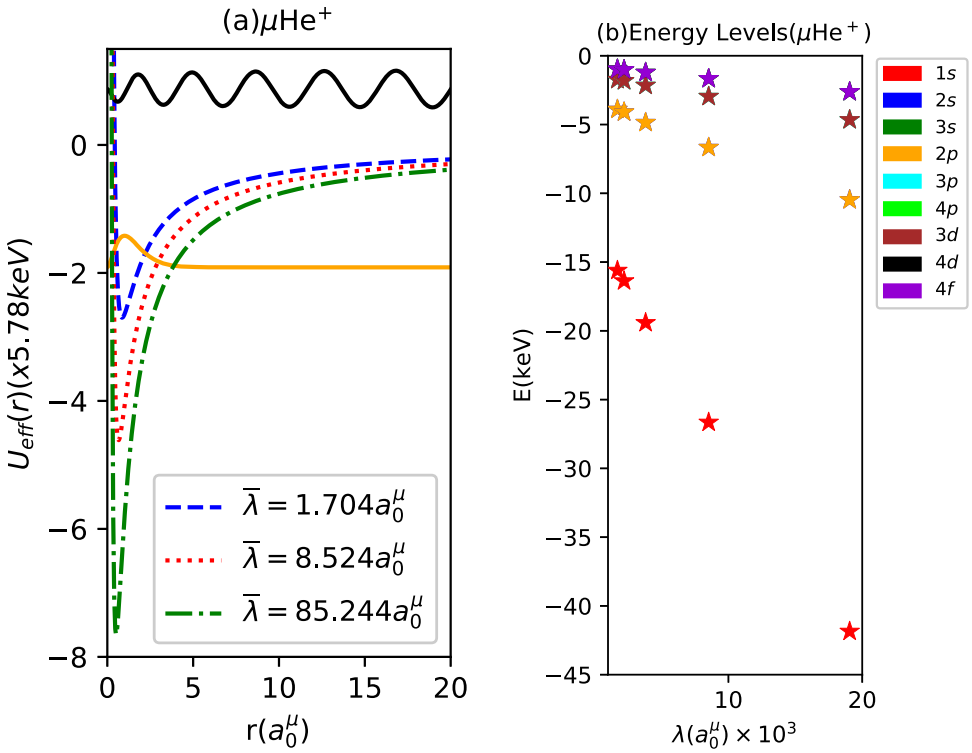

Fig. 3 Same as Fig. 1 but $(\mu\text{He})^+$

the bound state transitioning to the continuum state in a weakened effective potential shielded by NICP is higher. Therefore, the highest PCS value around the ionization threshold is observed for $\overline{\lambda} = 1.704a_0^\mu$. In Fig. 2b–d, the wave functions of the $1s$ and some pseudocontinuum states are shown for the corresponding $\overline{\lambda}$ value. The main reason for the characteristics of the PCS curves is the overlapping of the $1s$ and continuum wave functions, as long as there is no any scattering effect, in other words, the interference of these wave functions. The overlap of the outgoing photomuon waves with the $1s$ wave function closely affects the dipole oscillator strength density.

In Fig. 3a, the effective potential for $(\mu\text{He})^+$ embedded in a NICP environment with an impenetrable spherical radius of $R_0 = 20a_0^\mu$ is analyzed for three different λ values for $\ell = 1$. The $2p$ bound state wave function and a continuum state wave function with an energy of 6.793609 keV are synchronized with the potential, and these are for $\bar{\lambda} = 1.704a_0^\mu$. As seen in Fig. 3a, since the number of protons in the nucleus of the $(\mu\text{He})^+$ ion is greater than that in the muonic hydrogen atom, the attraction potential energy is also greater. Intense potential energy is observed in small ranges of the radial variable. In Fig. 3b, energy levels for some s, p, d, and f states of the $(\mu\text{He})^+$ ion are shown as a function of the plasma screening parameter λ. As observed, due to the significant attraction potential of the helium nucleus, all of these states are in the bound state. The plasma screening affects the $1s$ and $2p$ states more prominently compared to other states. This is because these levels are closer to the nucleus and feel the strong attraction energy most intensely within a smaller radial range. On the other hand, it is observed that states other than $1s$ and $2p$ are degenerate. While this condition provides stability and robustness to the system, it complicates the modeling and understanding of the system. Additionally, it makes the controllability of some spectroscopic and optical properties challenging. In Fig. 4a, the PCS curves of $(\mu\text{He})^+$ for four different values of the plasma shielding parameter λ and a free-plasma environment are shown as a function of the photomuon energy when $R_0 = 20a_0^\mu$. In Fig. 4b-d, the wave functions of the $1s$ and some pseudocontinuum states are exhibited for the corresponding $\overline{\lambda}$ value. For low values of the λ parameter, the NICP environment results in a weaker attraction effect, leading to relatively weaker binding energy of μ^- (see Fig. 3a). This facilitates the photoionization process. Therefore, around the ionization threshold, the PCS value is the highest for $\overline{\lambda} = 1.704a_0^\mu$ and lowest for the free-plasma environment. The characteristic of higher PCS values for lower values of λ converts around the $4 - 5$ keV photomuon energy range. In this range, the PCS value for $\overline{\lambda} = 19.061a_0^\mu$ (and also for the free-plasma) is higher than the PCS values for other $\overline{\lambda}$. As the photomuon energy increases for $\overline{\lambda} = 1.704 - 8.524a_0^\mu$, the PCS values decrease almost linearly, while for $\overline{\lambda}$ values beyond $8.524a_0^\mu$ and even in the Coulomb limit, the PCS values increase smoothly after the photomuon energy around 3 keV. The basis of this increment is that the muon in the $1s$ state is localized in both a deep and very narrow spatial location (see Fig. 4c). This localized state of the muon in this narrow region leads it to transition to higher-level continuum states after absorbing the necessary photon energy for photoionization. Because a muon localized in such a small spatial region also possesses a correspondingly great momentum, surpassing the threshold energy required to exit this small spatial location results in excess energy, aligning with the Heisenberg uncertainty principle. This results in a higher PCS value for the muon, which ascends to higher continuum levels with relatively great energy, an expected outcome. Another explanation for

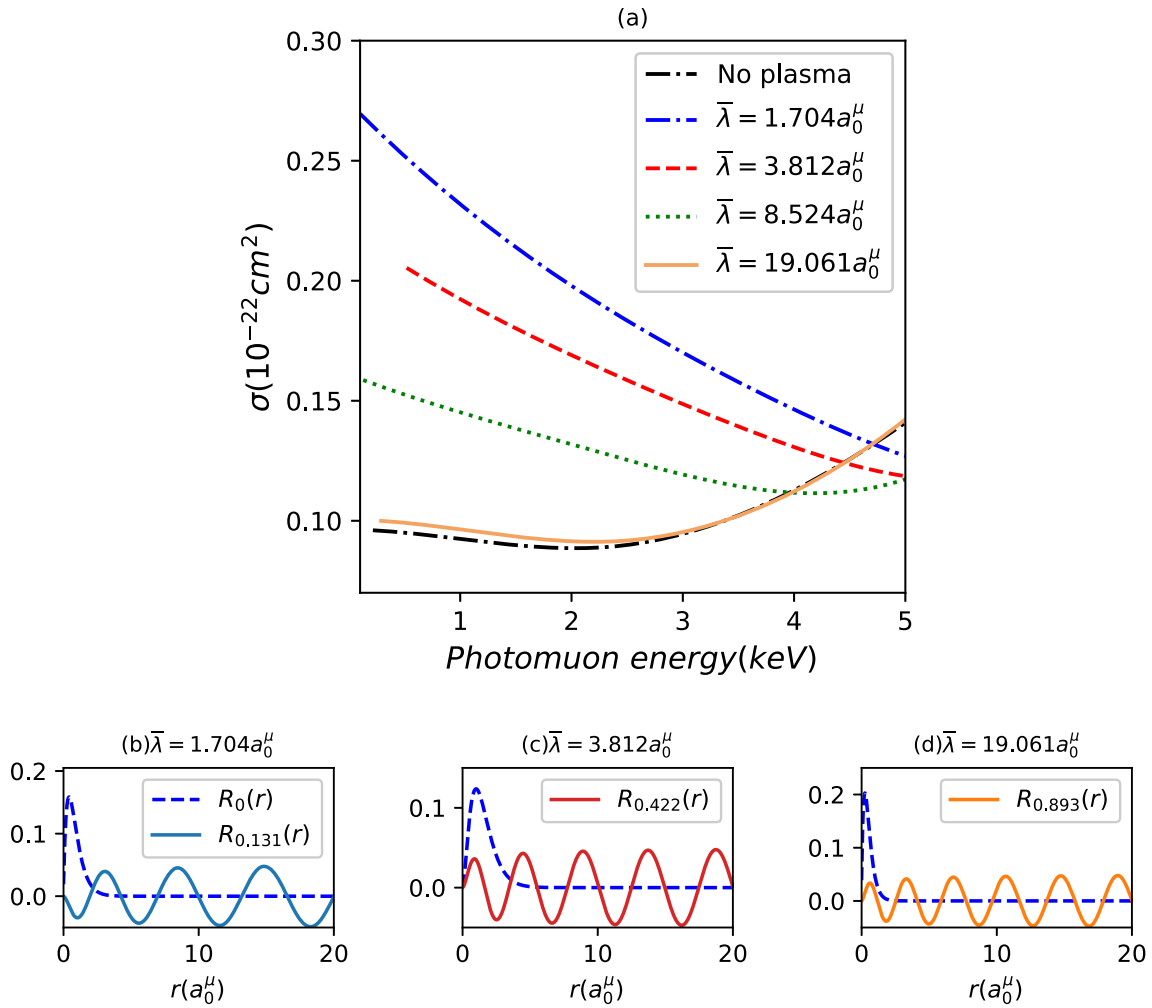

Fig. 4 Same as Fig. 2 but $(\mu\text{He})^+$

this result lies in the wave-like analysis of μ^-. The source of the relevant results, or in other words, the overlapping of the $1s$ and continuum state wave functions presented in Fig. 4b–d, accounts for this outcome.

In Fig. 5a, the effective potential profiles for $\ell = 1$ of $(\mu\text{Li})^{++}$ embedded in a NICP environment within a confining impenetrable spherical radius of $R_0 = 20a_0^\mu$ are plotted for three different λ values. At $\bar{\lambda} = 1.704a_0^\mu$, the potential includes a $2p$ bound state wave function and a continuum state wave function with an energy of 5.432366 keV, representing the relevant potential profile data. As observed in the potential panel, the attraction potential energy of the $(\mu\text{Li})^{++}$ ion on μ^- is approximately twice that of $(\mu\text{He})^+$ ion. An increase in the λ parameter enhances the strength of the $U_{\text{eff}}(r)$ potential. Due to the relatively higher proton count in the Li nucleus, the potent confinement effect of the potential occurs in a much narrower spatial region within the Li nucleus. In Fig. 5b, the energy levels for some s, p, d, and f states of $(\mu\text{Li})^{++}$ ion are provided as a function of the λ plasma screening parameter. As observed, all energy levels of μ^- due to the Li nucleus are in a bound state, rendering the system more stable with additional bound state energy values compared to the other two muonic systems. An increase in λ typically results in a deepening potential, which is expected to cause a lowering of bound states. The $1s$ and $2p$ levels are the most affected by this lowering, while degeneracy is observed in levels other than them. In Fig. 6a, when $R_0 = 20a_0^\mu$, the PCS curves of $(\mu\text{Li})^{++}$ are provided as a function of the photomuon energy for four different values of the plasma shielding parameter λ and for the free-plasma environment. In Fig. 6b-d, the wave functions of $1s$ and some pseudocontinuum states are presented for the respective $\bar{\lambda}$ value. At low values of λ, where

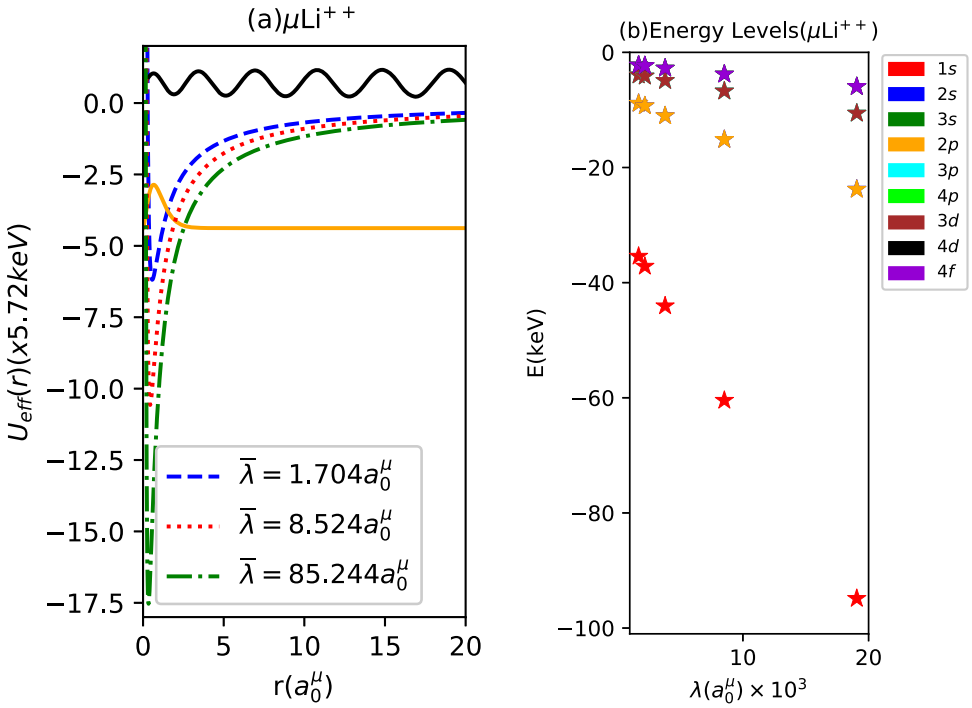

Fig. 5 Same as Fig. 1 but $(\mu Li)^{++}$

the attractiveness of the atomic system's $U_{\text{eff}}(r)$ potential is relatively lower, it is easier to convert the weakly bound μ^- into a photomuon, hence the likelihood of this event occurring is higher. Therefore, as the λ value increases, it becomes more difficult to remove the muon from the deepening potential by the photon, while the PCS values are small at large values of λ around the ionization threshold, while the PCS values are large at small λ values (see Fig. 6a). As observed in Fig. 6a, except for the PCS curve at $\bar{\lambda} = 8.524a_0^\mu$, the other PCS curves exhibit a rather monotonic decrease up to a certain photon energy, beyond which they noticeably increase. However, this behavior is exhibited by the $(\mu He)^+$ ion only for $\bar{\lambda} = 19.061a_0^\mu$ and the free-plasma case (see Fig. 4a). This difference arises because the $(\mu He)^+$ ion reached a very narrow spatial localization state at small λ values (Fig. 3a). On the other hand, the $(\mu Li)^{++}$ ion, due to the additional protons in its nucleus alongside the plasma effect, is more effective in achieving spatial localization within a narrow range. From such a narrow and deep spatial region, the muon, by absorbing photons, can ascend to higher continuum levels with its high kinetic energy, which aligns with the Heisenberg uncertainty principle. The absorption process and the situation of having high energy increase the likelihood of photomuon formation, thereby increasing the PCS values, as can be seen in Fig. 6a. Essentially, the dynamics of this process, i.e., the depth of the potential and the localization states, are reflected in the bound and pseudocontinuum wave functions, as seen in Fig. 6b-d. The overlap of bound-pseudocontinuum state wave functions constitutes the fundamental dynamics of this process. The different character of the PCS curve for $\bar{\lambda} = 8.524a_0^\mu$ (exhibiting a decrease approximately after 3 keV photomuon energy) is due to this mentioned dynamic. In summary, in the case of $\bar{\lambda} = 8.524a_0^\mu$, the wave function of the muon localized at a specific point in the potential, and due to this characteristic, the energy obtained after photon absorption and ionization, as well as the different overlapping conditions, can lead to observed different PCS characteristics.

In Fig. 7a, the effect of confinement on the PCS of the μH atom embedded in the NICP is investigated. As expected, as the confinement radius R_0 decreases, all energy levels rise. In every scenario, while PCS values are maximum around the ionization threshold of the μH atom, they decrease as the photon energies increase (see Fig. 7a-d). Because the bound states of the muon are more unstable at small R_0 values, photomuon energies are higher in small R_0 regimes and lower in large R_0 regimes, as seen in Fig. 7a–d. Both bound and pseudocontinuum states are affected by the strength of the spherical confinement. The probability of the muon being confined in such a narrow spatial zone being weak is reflected accordingly in the wave function (see Fig. 7e). The location and character of the 1*s* and continuum states shown in Fig. 7e–g are a dominant factor in determining the PCS. As

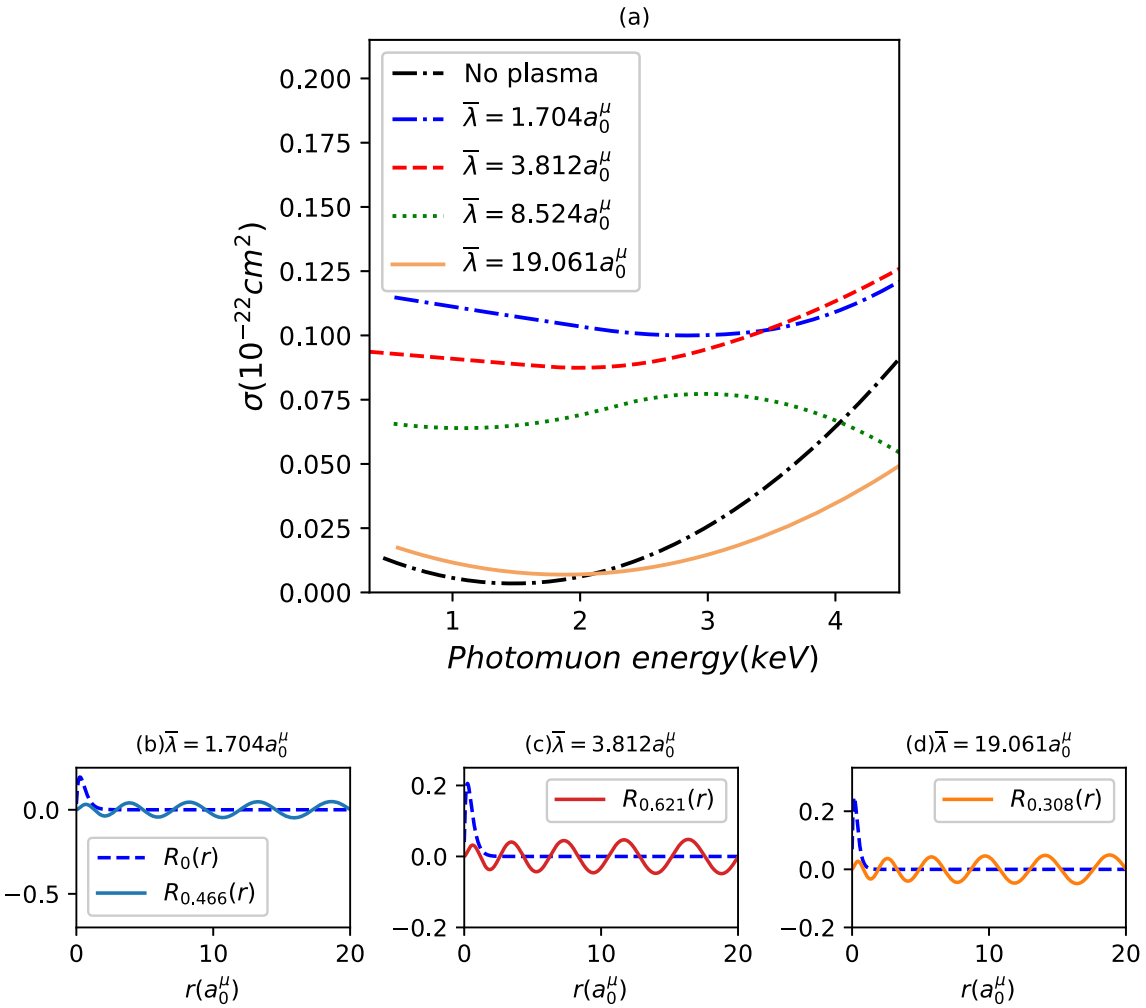

Fig. 6 Same as Fig. 2 but $(\mu\text{Li})^{++}$

seen in Fig. 8a–d, the response of the PCS of $(\mu\text{He})^+$ to R_0 is quite similar to that of μH atom. However, there is an increasing trend observed after $R_0 = 15a_0^\mu$ (see Fig. 8c). This is because, due to the stronger attraction energy of the He nucleus compared to hydrogen, the muon localized in a narrow region of the effective potential absorbs photon energy and reaches higher energies after ionization. This results in a greater PCS value and a higher photomuon energy. The stronger attraction potential of the $(\mu\text{He})^+$ ion compared to the μH atom has created a significant difference in the localization of the ground state (see comparison between Figs. 7e–g and 8e–g). The wave characteristics of bound-pseudocontinuum wave functions are very effective on PCSs. As observed in Fig. 9a–d, similar results are seen within $(\mu\text{Li})^{++}$. When $R_0 = 3.5$ and $5a_0^\mu$, the muon is more unstable and easily excited. In such cases, it is evident that higher photomuon energies can be observed upon absorbing a high-energy photon (see Fig. 9a, b). Compared to μH and $(\mu\text{He})^+$, the nucleus of $(\mu\text{Li})^{++}$ has the strongest attraction potential. It also produces a very narrow confinement range, especially for the ground state, as can also be seen in Fig. 5a. In such a narrow region, it is common for a muon in the bound state to have higher energy after ionization upon absorbing a photon. The PCS, which is a measure of the likelihood of this event occurring, is related to the overlap of the wave functions shown in Fig. 9e–g.

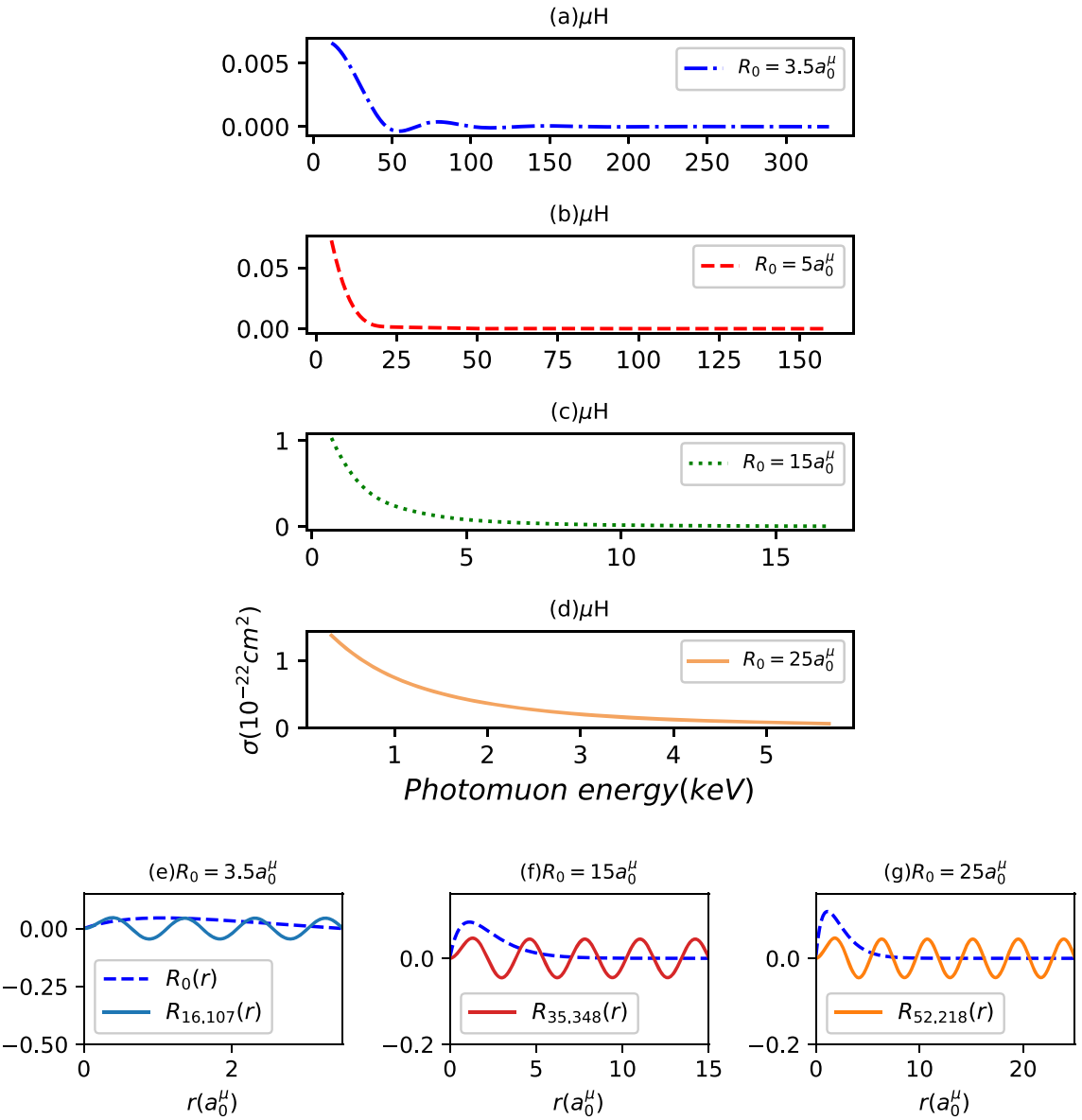

Fig. 7 **a–d** Photoionization cross sections for μH atom immersed in the non-ideal classical plasma with $\bar{\lambda} = 19.061a_0^\mu$, as a function of photomuon energy, respectively, for $R_0 = 3.5$, 5, $15a_0^\mu$ and $25a_0^\mu$. **e**, **f** and **g** The radial wave functions for $1s-$state and continuum states for $R = 3.5$, 15, $25a_0^\mu$ as a function of r, where E_n for $R_{E_n}(r)$ is in muonic atomic units (m.a.u.)

In Fig. 10, the PCS characteristics of μH, $(\mu\text{He})^+$, and $(\mu\text{Li})^{++}$ embedded in Debye, quantum, and NICP environments are shown as a function of photomuon energy. Considering the Debye and quantum plasma (QP) potentials in Eqs. 24 and 25 was sufficient for the calculations. The PCS response of all three atomic systems to plasmas exhibits similar characteristics, decreasing with increasing photomuon energy. The functionality of Debye and quantum plasmas on the PCS is almost identical. However, the NICP environment results in a noticeable difference in the PCS data. This indicates that compared to Debye and quantum plasmas, the NICP may be a more effective alternative for the dynamics of muon's PCS. Especially in the cases of He and Li, the NICP data provides more distinct responses to photomuon energy, as seen in Fig. 10a-c.

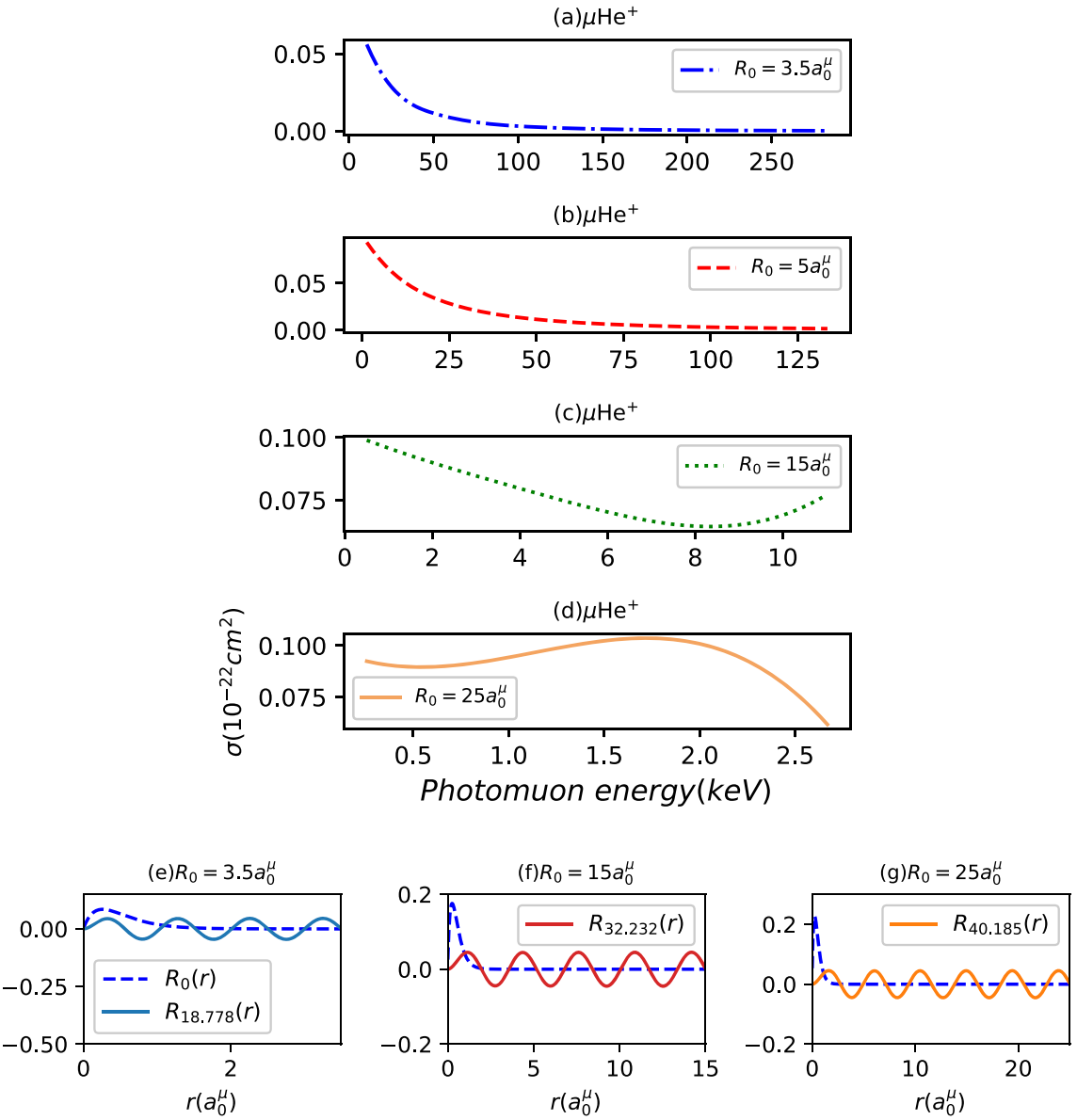

Fig. 8 Same as Fig. 7 but $(\mu He)^+$

4 Concluding remarks

The PCS analysis of μH, $(\mu He)^+$, and $(\mu Li)^{++}$ systems in a spherical confinement within the NICP environment has been conducted. The increase in the plasma screening parameter λ in the NICP enhances the effective potential attractiveness in all three systems, making the system more stable. Degeneracy is observed in levels other than $1s$ and $2p$ in $(\mu He)^+$ and $(\mu Li)^{++}$ ions. Particularly, degeneracy becomes significant in situations such as chemical reactions, magnetic properties, or spectroscopic analyses. To eliminate the observed degeneracy in He and Li, the external influences such as the laser pulses, electric, or magnetic fields can be applied. This is because it has been determined that increasing or decreasing the confinement radius R_0 does not eliminate this degeneracy. However, due to the nuclear attraction potential, the systems in the plasma environment are ranked in terms of stability as $(\mu Li)^{++}$, $(\mu He)^+$, μH. Since there is no scattering center or effect in the system, the confinement or copper resonance peaks are not observed

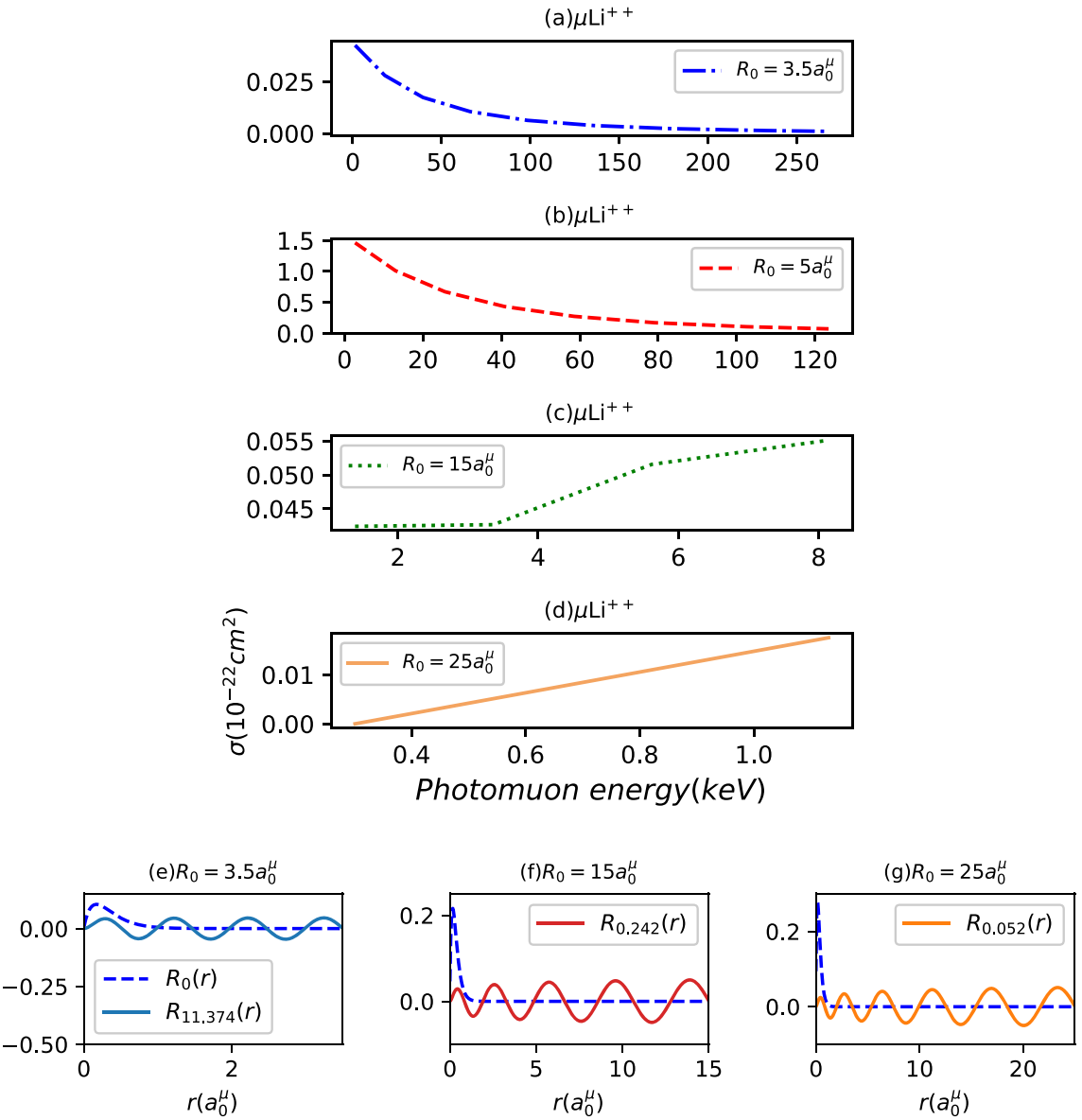

Fig. 9 Same as Fig. 7 but $(\mu Li)^{++}$

in the PCS curves. We can characterize the PCS curves as the spectral distribution of ionization probability. The localized nature of the bound states of these exotic systems within a very narrow region of the effective potential leads to high photomuon energies and high PCS values after photon absorption occurs. Therefore, as we progress from muonic hydrogen to muonic lithium, a rising trend in PCS curves emerges starting from smaller photomuon energies. The reasons for the characteristics of PCS are heavily influenced by the overlapping of bound and continuum wave functions. The decrease in the confinement radius R_0 renders the system's muons unstable. The nuclear potential energies, and thus the boundaries of spatial localization, are the main factors in the analysis of R_0, contributing to the formation of high photomuon energies and high PCS values. Of course, this main factor is either reinforced or weakened by the NICP environment, which is evident in the results. In this context, it has been determined that the NICP would be a

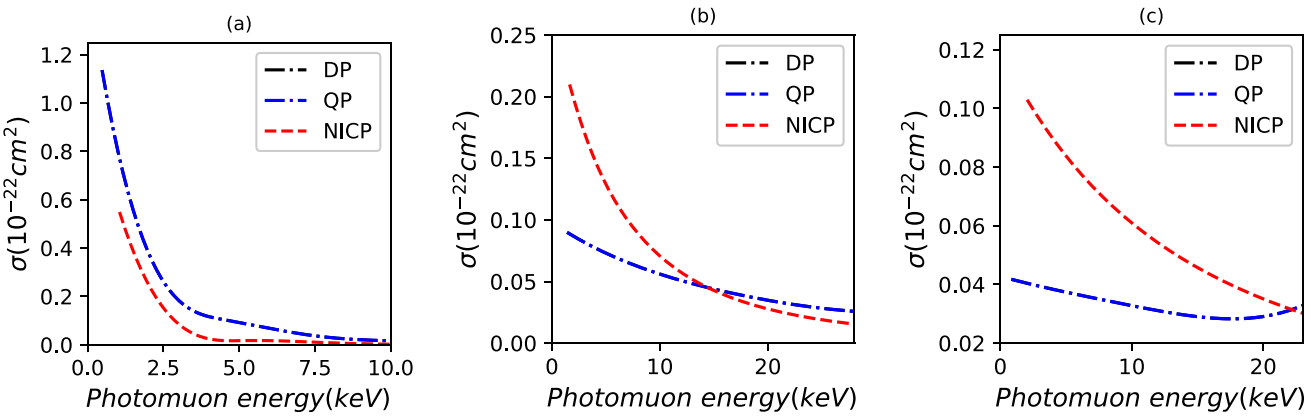

Fig. 10 Photoionization cross sections of **a** μH, **b** $(\mu\text{He})^+$ and **c** $(\mu\text{Li})^{++}$ immersed in the Debye, quantum and non-ideal classical plasma, when $\bar{\lambda} = 1.704a_0^\mu$ and $R_0 = 10a_0^\mu$, as a function of photomuon energy

more effective mechanism compared to Debye and quantum plasmas for the photoionization treatments of μH, $(\mu\text{He})^+$, and $(\mu\text{Li})^{++}$ systems. Despite the muon's short lifetime, understanding PCS processes can lead to significant results in various applications and fundamental scientific research. The findings of our work provide a valuable contribution to gaining a deeper understanding of plasma physics and atom-photon interactions and guiding future experimental studies. Therefore, despite the muon's short lifetime, we can provide a significant contribution to the scientific community with the results of this research.

Funding Open access funding provided by the Scientific and Technological Research Council of Türkiye (TÜBİTAK).

Availability of data and material The datasets generated during and/or analyzed during the current study are available from the corresponding author on reasonable request.

Declarations

Conflict of interest Mustafa Kemal Bahar is the only author in the study.

References

1. N.J. Clayden, Muons in chemistry. Phys. Scr. **88**, 067507 (2013)
2. S. Ito, Muon spin rotation/resonance (μSR) for studying radical reactivity of unsaturated organophosphorus compounds. Chem.-A Eur. J. **28**(53), e202200843 (2022)
3. J.S. Cohen, Isotope effects on antiproton and muon capture by hydrogen and deuterium atoms and molecules. Phys. Rev. A **59**(2), 1160 (1999)
4. A.D. Hillier et al., Muon spin spectroscopy. Nat. Rev. Methods Prim. **2**, 4 (2022)
5. S.L. Lee, R. Cywinski, S.H. Kilcoyne, *Muon Science: Muons in Physics, Chemistry and Materials*, vol. 51 (CRC Press, Boca Raton, 1999)
6. A. Yaouanc, P.D. De Reotier, *Muon spin rotation, relaxation, and resonance: applications to condensed matter*, vol. 147 (OUP, Oxford, 2011)
7. S. Blundell, R. De Renzi, T. Lancaster, F.L. Pratt, *Muon Spectroscopy: An Introduction* (Oxford University Press, Oxford, 2022)
8. V.W. Hughes, C.S. Wu, *Muon Physics*, Weak Interactions, vol. II. (Academic Press, Cambridge, 1975)
9. D.G. Fleming, I. McKenzie, P.W. Percival, *Muon Spin Spectroscopy: Methods and Applications in Chemistry and Materials Science* (Wiley, Hoboken, 2024)
10. Y. Mori, Enforced stripping of negative muons from μHe^+ ions to stimulate muon-catalyzed fusion by cyclotron resonance acceleration. Prog. Theor. Exp. Phys. **9**, 093G01 (2021)
11. S.F.J. Cox, *Muon Spin Spectroscopy: Basics, Techniques, and Applications* (Oxford University Press, Oxford, 2011)
12. S. Chelkowski, A.D. Bandrauk, P.B. Corkum, Muonic molecules in superintense laser fields. Phys. Rev. Lett. **93**(8), 083602 (2004)
13. V. Aquilanti, H.E. Montgomery, C.N. Ramachandran, N. Sathyamurthy, Atoms and molecules in a confined environment. Eur. Phys. J. D **75**, 187 (2021)
14. K.S. Khaw, A. Antognini, T. Prokscha, K. Kirch, L. Liszkay, Z. Salman, P. Crivelli, Spatial confinement of muonium atoms. Phys. Rev. A **94**(2), 022716 (2016)
15. R.A. Rojas, N. Aquino, A. Flores-Riveros, J.F. Rivas-Silva, Confined muonic hydrogen-like atoms. Eur. Phys. J. D **75**, 116 (2021)

16. X.Y. Fu, Z. Jiang, S. Kar, The ^{3} P_0 states of exotic molecular ions with exponential-cosine-screened coulomb potentials. Few-Body Syst. **64**, 15 (2023)
17. A.M. Frolov, Atomic few-body systems with muonium. J. Phys. B: At. Mol. Opt. Phys. **50**, 105102 (2017)
18. R. Pohl et al., Observation of long-lived muonic hydrogen in the 2s state. Phys. Rev. Lett. **97**, 193402 (2006)
19. P. Amaro et al., Laser excitation of the 1s-hyperfine transition in muonic hydrogen. SciPost Phys. **13**(2), 020 (2022)
20. A. Poszwa, M.K. Bahar, A. Soylu, The nuclear size and mass effects on muonic hydrogen-like atoms embedded in Debye plasma. Phys. Plasmas **23**, 103515 (2016)
21. A.N. Sil, B. Saha, P.K. Mukherjee, Effect of Debye plasma on compressed exotic atoms. Phys. Lett. A **324**, 308 (2004)
22. A.N. Sil, M. Pawlak, P.K. Mukherjee, M. Bylickib, The influence of Debye plasma on the ground state energies of exotic systems. J. Quant. Spectrosc. Radiat. Transf. **109**, 873 (2008)
23. S. Bhattacharyya, A.N. Sil, T.K. Mukherjee, P.K. Mukherjee, P. Vasu, Electron affinity of exotic systems under Debye plasma. Int. J. Quantum Chem. **107**, 946 (2007)
24. S. Kar, Y.K. Ho, Bound states and resonance states of the plasma-embedded $td\mu$ and $dd\mu$ molecular ions. Eur. Phys. J. D **48**, 157 (2008)
25. V.E. Fortov, I.T. Iakubov, *The Physics of Nonideal Plasma* (World Scientific, Singapore, 2000)
26. D. Zubarev, V. Morozov, G. Röpke, *Statistical Mechanics of Nonequilibrium Processes, in Basic Concepts, Kinetic Theory*, vol. 1 (Akademie Verlag, Belin, 1996)
27. V.E. Fortov, T.I. Igor, *The Physics of Nonideal Plasma* (World Scientific, Singapore, 2000)
28. K.D. Sen, K. Kumar, C. Yadav, V. Prasad, Multipole polarizabilities and dipole oscillator strengths of H-atom in nonideal classical plasmas. Eur. Phys. J. Plus **137**, 78 (2022)
29. Z. Jiang, S. Kar, Polarizabilities of the negative ions of hydrogen and positronium in nonideal classical plasmas. Phys. Plasmas **31**, 012105 (2024)
30. N. Das, B. Das, A. Ghoshal, Spherically confined hydrogenic atoms under classical nonideal plasmas: scaling law for the critical cage size. Int. J. Quant. Chem. **124**, e27265 (2024)
31. Z.B. Chen, Study of atomic spectroscopy and electron collision process in nonideal classical plasmas. Physics Plasmas **30**, 052105 (2023)
32. M.K. Bahar, Li@C_n immersed in nonideal classical plasmas. Eur. Phys. J. Plus **137**(9), 1076 (2022)
33. M.K. Bahar, C. Martinez-Flores, Photoionization cross section for H@C_n implanted in nonideal classical plasmas. Ann. Phys. **535**, 2300188 (2023)
34. F.B. Baimbetov, Kh.T. Nurekenov, T.S. Ramazanov, Pseudopotential theory of classical nonideal plasmas. Phys. Lett. A **202**, 211 (1995)
35. B.N. Datta, *Numerical Linear Algebra and Applications*, 2nd edn. (SIAM, Philadelphia, 2010)
36. A. Messiah, *Quantum Mechanics* (Elsevier, Amsterdam, 1961)
37. H.A. Bethe, E.E. Salpeter, *Quantum Mechanics of One and Two-Electron Atoms* (Plenum, Edison, 1977)
38. L.M. Ugray, R.C. Shiell, Elucidating Fermi's golden rule via bound-to-bound transitions in a confined hydrogen atom. Am. J. Phys. **81**, 216 (2013)
39. S. Kar, Y.K. Ho, Bound states and resonance states of the plasma-embedded $pp\mu$ molecular ion. Phys. Rev. A **75**, 062509 (2007)